Partial-wave analysis of $\vec{p}\vec{p} \to pp\pi^0$ data

P. N. Deepak,* J. Haidenbauer,† and C. Hanhart
Institut für Kernphysik (Theorie), Forschungszentrum Jülich, 52428 Jülich, Germany
(Received 5 April 2005; published 31 August 2005)

We present a partial-wave analysis of the polarization data for the reaction $\vec{p}\vec{p} \to pp\pi^0$, based solely on the recent measurements at the Indiana University Cyclotron Facility for this channel. Methods for an improved analysis are discussed. We compare the extracted values to those from a meson exchange model. The fit leads to a χ^2 per degree of freedom of 1.7.

DOI: 10.1103/PhysRevC.72.024004 PACS number(s): 25.10.+s, 24.70.+s, 13.75.Cs, 25.40.Qa

I. INTRODUCTION

Understanding pion production in nucleon–nucleon (NN) collisions near threshold is of high theoretical interest for various reasons. As the first strong inelasticity for the NN system, its phenomenology is closely linked to that of elastic NN scattering (for recent reviews on the subject of near-threshold pion production see Refs. [1,2]). In addition, as the pion is a Goldstone boson of the chiral symmetry of strong interactions, its dynamics is strongly constrained by this symmetry (see Ref. [3] and references therein). Recently a scheme was discussed that is said to lead to a convergent effective field theory even for large momentum transfer reactions such as $NN \to NN\pi$ [4,5]. Confirmation of this claim is the precondition for a successful analysis of the isospin-violating pion production reactions measured recently, namely, the forward–backward asymmetry in $pn \to d\pi^0$ [6] and the total cross-section measurement for $dd \to \alpha\pi^0$ [7].

A complete set of polarization observables for the reaction $\vec{p}\vec{p} \to pp\pi^\circ$ was measured for the first time in 2001 [8]. Of the two existing advanced models of pion production in NN collisions [9,10] that include higher partial waves and therefore allow predictions for polarization observables, only the model of the Jülich group [9,11] has been thoroughly confronted with those data. It turned out that this model failed to provide an overall satisfactory reproduction of these polarization observables [8,12]. On the other hand, the (less complete) data for $\vec{p}\vec{p} \to pn\pi^+$ [13] as well as those for $\vec{p}\vec{p} \to d\pi^+$ [14] were described very well by the same model. So far the reasons for the shortcoming of this phenomenological model in describing the neutral pion production—while being rather successful for the charged pions—is not yet understood.[1]

The presence of spin leads to contributions of many partial-wave amplitudes, even close to threshold, which is the regime of interest here. It is thus difficult to draw any more concrete conclusion from a comparison of the model results directly with the data. It is well known that a partial-wave analysis is an important intermediate step toward an understanding of hadronic reactions: being in principle equivalent to the full data set, the partial–wave amplitudes can be much more easily interpreted in terms of their physics content. As a consequence, a comparison of the theoretical results with the partial-wave amplitudes is expected to reveal the strengths or weaknesses of the theory much more clearly than a direct comparison with the data.

In this paper we present a first step toward a full partial-wave decomposition of the reaction $pp \to pp\pi^0$. In our work we use as input only data from the recent Indiana University Cyclotron Facility (IUCF) measurement [8]. However, as will be stressed below, a combined analysis of both the production data and the data on elastic pp scattering is certainly desirable for the future. In [8], the various angular-dependent structures of the polarization observables were fitted under particular assumptions about the partial-wave content of the data as well as about the energy dependence of some of the amplitudes. Since we consider these assumptions, which were necessitated by the limited statistical accuracy of the data, to be reasonable and plausible, we adopt them for our analysis, too. This also has the advantage that we can use the extracted coefficients of Ref. [8] directly in our fitting procedure. In any case, starting from the same limited number of partial-wave amplitudes, we would expect to arrive at the same values for the extracted parameters.

This paper is organized as follows: in the next section we will describe the theoretical formalism that allows one to relate the observables to the partial-wave amplitudes. In Sec. III the method of extraction as well as that for determining the uncertainties are explained. Then, in Sec. IV we discuss the results and compare them with those of a microscopic model [9]. The paper closes with a short summary and a discussion of further steps.

II. THEORETICAL FORMALISM

The $\boldsymbol{T}$ matrix for $pp \to pp\pi^0$ may be expressed in the form [15]

$$\boldsymbol{T} = \sum_{s_f,s_i=0}^{1} \sum_{\lambda=|s_i-s_f|}^{s_i+s_f} [S^\lambda(s_f,s_i)\cdot T^\lambda(s_f,s_i)], \qquad (1)$$

*Present address: Physics Group, Birla Institue of Technology and Science, Pilani-Goa Campus, Zuarinagar-403726, Goa, India.
†Corresponding author; electronic address: j.haidenbauer@fz-juelich.de.

[1]Note, however, that effective field theory studies revealed many conceptual problems in this approach, as discussed in [2]; it is up to now unclear how much impact those have on the description of the observables.

where s_i, s_f denote the initial and final channel spins, respectively. We use the same notation as in [16], where the irreducible channel-spin transition operators $S^{\lambda}_{m_\lambda}(s_f, s_i)$ of rank λ are defined. If in the c.m. $\vec{p}_i$, $\vec{p}$ denote the relative momenta of the two protons in the initial and final states and $\vec{q}$ the momentum of the pion, the irreducible tensor reaction amplitudes $T^{\lambda}_{m_\lambda}(s_f, s_i)$ in Eq. (1) can be expressed in the form [15]

$$T^{\lambda}_{m_\lambda}(s_f, s_i) = \sum_{L_p, L, l_q} \sum_{j, J, L_f} (-1)^{L_f} [j][L_f][J]^2 [s_f]^{-1} \times \begin{Bmatrix} s_f & L_f & J \\ L & s_i & \lambda \end{Bmatrix} \begin{Bmatrix} s_f & L_p & j \\ l_q & J & L_f \end{Bmatrix} T^{J}_{l_q(L_p s_f) j; L s_i} \times \{[Y_{L_p}(\hat{p}) \otimes Y_{l_q}(\hat{q})]^{L_f} \otimes Y_L(\hat{p}_i)\}^{\lambda}_{m_\lambda} \quad (2)$$

to separate the energy and angular dependences of the amplitudes. In Eq. (2), we use the shorthand notation $[j] = \sqrt{2j+1}$, and $(T_1 \otimes T_2)^L_m$ indicates the coupling of the two irreducible tensors T_1 and T_2 to total angular momentum L with projection m. The partial-wave amplitudes $T^{J}_{l_q(L_p s_f) j; L s_i}$ are functions of both the c.m. energy $E_{\text{c.m.}}$ and ϵ, the relative kinetic energy of the nucleon pair in the final state (in contrast to a two-body reaction, where the partial-wave amplitudes are characterized by a single energy variable).

If $\vec{P}$, $\vec{Q}$ denote, respectively, the beam and the target polarizations, the differential cross section in a double-polarized experiment may be written as [15]

$$\frac{d\sigma}{d\Omega_p d\Omega_q d\epsilon} = \frac{1}{4} \sum_{k_1, k_2 = 0}^{1} \sum_{k = |k_1 - k_2|}^{k_1 + k_2} [(P^{k_1} \otimes Q^{k_2})^k \cdot B^k(k_1, k_2)], \quad (3)$$

in terms of the irreducible tensors

$$B^k_\nu(k_1, k_2) = 2(-1)^{k_1 + k_2} [k_1][k_2] \sum_{s_f = 0}^{1} (2 s_f + 1) \times \sum_{s_i, s_i' = 0}^{1} \sum_{\lambda, \lambda'} (-1)^{s_i' + s_f} [s_i][s_i'][\lambda][\lambda'] \times \begin{Bmatrix} s_i' & s_i & k \\ \lambda & \lambda' & s_f \end{Bmatrix} \begin{Bmatrix} \frac{1}{2} & \frac{1}{2} & s_i \\ \frac{1}{2} & \frac{1}{2} & s_i' \\ k_1 & k_2 & k \end{Bmatrix} [T^{\lambda}(s_f, s_i) \otimes T^{\dagger^{\lambda'}}(s_f, s_i')]^k_\nu, \quad (4)$$

which are bilinear in the irreducible tensor amplitudes $T^{\lambda}_{m_\lambda}(s_f, s_i)$, whose complex conjugates $T^{\lambda}_{m_\lambda}(s_f, s_i)^*$ define $T^{\dagger^{\lambda}}_{m_\lambda}(s_f, s_i) = (-1)^{m_\lambda} T^{\lambda}_{-m_\lambda}(s_f, s_i)^*$. If

$$\sigma_0(\xi) = \tfrac{1}{4} B^0_0(0, 0) \quad (5)$$

denotes the unpolarized differential cross section with ξ collectively standing for $\{\hat{p}, \hat{q}, \epsilon\}$, the $B^k_\nu(k_1, k_2)$ are related to the independent (Cartesian) spin observables $A_{ij}(\xi)$, defined in [8], through

$$\sigma_0(\xi)\, A_{y0}(\xi) = \tfrac{-1}{2\sqrt{2}}\, \Im\big[B^1_1(1,0)\big], \quad (6a)$$

$$\sigma_0(\xi)\, A_{xz}(\xi) = \tfrac{1}{4}\big\{\Re\big[B^1_1(1,1) - B^2_1(1,1)\big]\big\}, \quad (6b)$$

$$\sigma_0(\xi)\, A_{\Sigma}(\xi) = \tfrac{-1}{2\sqrt{3}}\big[B^0_0(1,1) + \tfrac{1}{\sqrt{2}} B^2_0(1,1)\big], \quad (6c)$$

$$\sigma_0(\xi)\, A_{zz}(\xi) = \tfrac{-1}{4\sqrt{3}}\big[B^0_0(1,1) - \sqrt{2} B^2_0(1,1)\big], \quad (6d)$$

$$\sigma_0(\xi)\, A_{\Delta}(\xi) = \tfrac{1}{2}\Re\big[B^2_2(1,1)\big], \quad (6e)$$

$$\sigma_0(\xi)\, A_{z0}(\xi) = \tfrac{1}{4} B^1_0(1,0), \quad (6f)$$

$$\sigma_0(\xi)\, A_{\Xi}(\xi) = \tfrac{-1}{2\sqrt{2}}\, \Im\big[B^1_0(1,1)\big]. \quad (6g)$$

TABLE I. Partial-wave amplitudes that could contribute to $\vec{p}\,\vec{p} \to pp\pi^0$ near threshold. Only contributions arising from the first 12 amplitudes were considered in the present analysis.

No.	Type	Our notation $T^J_{l_q(L_p s_f) j; L s_i}$	Notation of Meyer *et al.* [8] ${}^{2s_i+1}L_J \to {}^{2s_f+1}L_{pj}, l_q$
1	Ss	$T^0_{0(00)0;11}$	${}^3P_0 \to {}^1S_0, s$
2	Ps	$T^0_{0(11)0;00}$	${}^1S_0 \to {}^3P_0, s$
3		$T^2_{0(11)2;20}$	${}^1D_2 \to {}^3P_2, s$
4	Pp	$T^0_{1(11)1;11}$	${}^3P_0 \to {}^3P_1, p$
5		$T^2_{1(11)1;11}$	${}^3P_2 \to {}^3P_1, p$
6		$T^2_{1(11)2;11}$	${}^3P_2 \to {}^3P_2, p$
7		$T^2_{1(11)1;31}$	${}^3F_2 \to {}^3P_1, p$
8		$T^2_{1(11)2;31}$	${}^3F_2 \to {}^3P_2, p$
9		$T^1_{1(11)0;11}$	${}^3P_1 \to {}^3P_0, p$
10		$T^1_{1(11)1;11}$	${}^3P_1 \to {}^3P_1, p$
11		$T^1_{1(11)2;11}$	${}^3P_1 \to {}^3P_2, p$
12		$T^3_{1(11)2;31}$	${}^3F_3 \to {}^3P_2, p$
13	Sd	$T^2_{2(00)0;11}$	${}^3P_2 \to {}^1S_0, d$
14		$T^2_{2(00)0;31}$	${}^3F_2 \to {}^1S_0, d$
15	Ds	$T^2_{0(20)2;11}$	${}^3P_2 \to {}^1D_2, s$
16		$T^2_{0(20)2;31}$	${}^3F_2 \to {}^1D_2, s$

III. EXTRACTION OF PARTIAL-WAVE AMPLITUDES

A priori, a set of 16 partial-wave amplitudes can be expected to contribute to the reaction. We list them in Table I, explicitly both in our notation and the notation of Meyer *et al.* [8]. But we consider only contributions from the first 12 amplitudes, since final states with orbital angular momentum greater than 1 were ignored in the analysis of Meyer *et al.* [8]. Thus there are 24 real unknowns (12 complex amplitudes) to be determined. However, as overall phases are unobservable and as $s_f = 0$ and $s_f = 1$ *NN* final states do not mix with each other in any of the spin observables measured in [8] (final state polarizations were not measured), we have the freedom to choose the first two amplitudes to be real. This leaves 22 real numbers to be determined. Equations (11a)–(11h) of Ref. [8] represent the general angular dependence of $\sigma_0(\xi)$ and $\sigma_0(\xi) A_{ij}(\xi)$ in terms of the real coefficients E, F_k, G^{ij}_k, H^{ij}_k, I, K, I^{ij}, and K^{ij}. The quantities E, F_k, G^{ij}_k, and H^{ij}_k denote the weighted sums of bilinears in the partial-wave amplitudes corresponding, respectively, to $(\text{Ss})^2$, $(\text{Ps})^2$, (PsPp) and $(\text{Pp})^2$ interference terms, while I, I^{ij} and K, K^{ij} represent, respectively, the

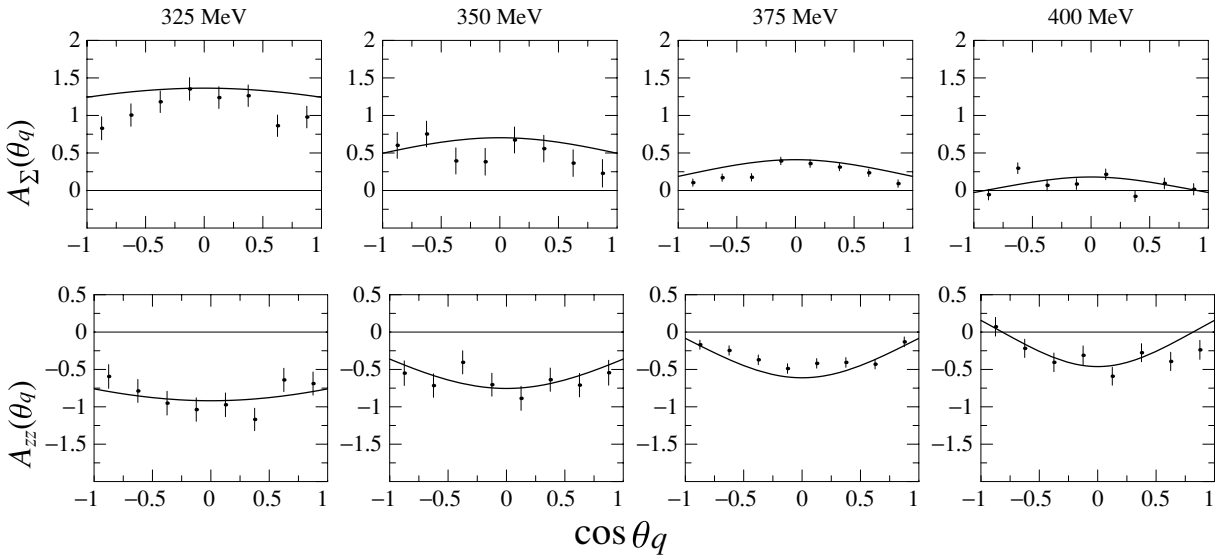

FIG. 1. The observables $A_\Sigma(\theta_q)$ and $A_{zz}(\theta_q)$ as a function of the pion angle at several bombarding energies. The data and the nomenclature for the observables are taken from Meyer *et al.* [8]. The solid curves represent our results.

contribution of (SsSd) and (SsDs) interference terms, which were ignored in the analysis of [8] and therefore also here. Using Eqs. (4) and (2), we obtain explicit expressions for all the observables in Eqs. (6a)–(6g), including the unpolarized differential cross section, defined in Eq. (5), in terms of the first 12 partial-wave amplitudes listed in Table I. These expressions, when compared with Eqs. (11a)–(11h) of [8], allow us to obtain explicitly the partial-wave decomposition of the coefficients E, F_k, G_k^{ij}, and H_k^{ij}.

Note that all values given in Table IV of Ref. [8] for the various coefficients are integrated with respect to the outgoing two-nucleon energy, ϵ. Thus, they are expressed as weighted sums of numerous $\mathcal{B}_{\kappa\kappa'}$, bilinear in the partial-wave amplitudes, as (we use nonrelativistic kinematics)

$$\mathcal{B}_{\kappa\kappa'}(E_{\text{c.m.}}) = \int_0^{\epsilon_{\max}} T_\kappa(E_{\text{c.m.}}, \epsilon) T^*_{\kappa'}(E_{\text{c.m.}}, \epsilon)\, q(E_{\text{c.m.}}, \epsilon) p(\epsilon)\, d\epsilon, \tag{7}$$

where T_κ, $\kappa = 2, \ldots, 12$, denotes the κth partial-wave amplitude listed in Table I (for example, $T_5(E_{\text{c.m.}}, \epsilon) \equiv T^2_{1(11)1;11}$), $p(\epsilon) = \sqrt{M_N \epsilon}$, and $q(E_{\text{c.m.}}, \epsilon) = \sqrt{2\mu(E_{\text{c.m.}} - 2M_N - m_\pi - \epsilon)}$, with the reduced mass of the outgoing three-body system $\mu = 2m_\pi M_N/(m_\pi + 2M_N)$, where M_N and m_π are the nucleon and pion masses, respectively. Thus, to proceed further we need to make an assumption regarding the ϵ dependence of the T_κ. In the

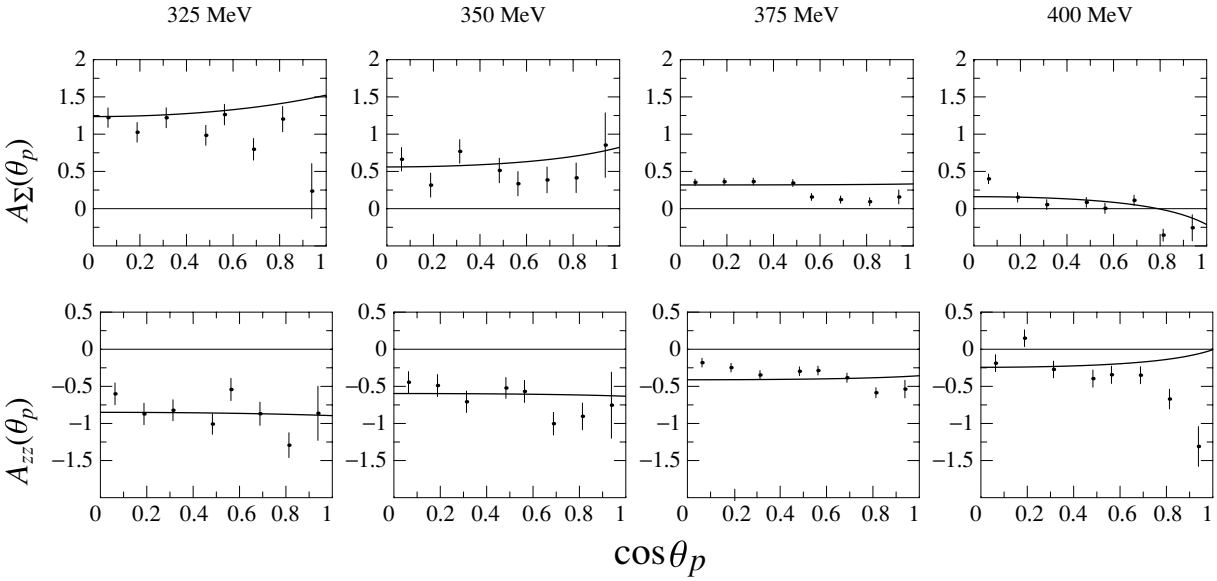

FIG. 2. The observables $A_\Sigma(\theta_p)$ and $A_{zz}(\theta_p)$ as a function of the proton angle at several bombarding energies. Same description of data and curves as in Fig. 1.

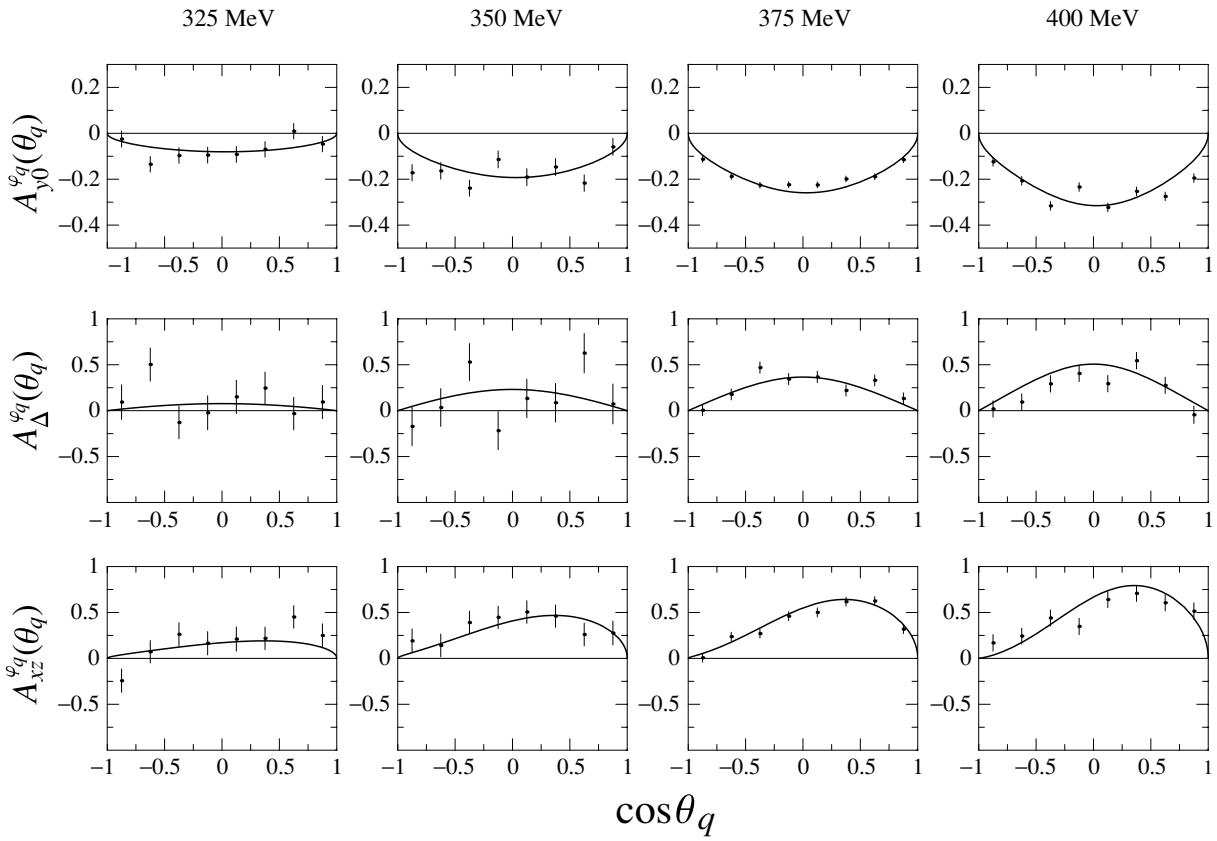

FIG. 3. The observables $A_{y0}^{\varphi_q}(\theta_q)$, $A_{xz}^{\varphi_q}(\theta_q)$, and $A_{\Delta}^{\varphi_q}(\theta_q)$ as a function of the pion angle at several bombarding energies. Same description of data and curves as in Fig. 1.

present first analysis of the IUCF data we use the most naive ansatz possible: we assume that the entire energy dependence of the amplitudes stems solely from the centrifugal barrier. This gives

$$T_\kappa(E_{\text{c.m.}}, \epsilon) \propto q(E_{\text{c.m.}}, \epsilon)^{l_q(\kappa)} p(\epsilon)^{L_p(\kappa)}, \tag{8}$$

which should hold as long as the outgoing momenta are small compared with the inverse of the production radius [17] and the effects of the final state interaction (FSI) are negligible. (This is obviously wrong for the *NN S* waves; they are discussed separately below.) Note that the same assumption was also used in the fitting procedure of Ref. [8] in order to determine some of the coefficients E, F_k, G_k^{ij}, and H_k^{ij} from the data, for the statistical accuracy of the data did not allow for a separate fit of these coefficients at each energy. From the ansatz of Eq. (8), one easily derives [18]

$$\mathcal{B}_{\kappa\kappa'}(E_{\text{c.m.}}) = z_\kappa\, z_{\kappa'}^*\, \eta^{l_q(\kappa)+l_q(\kappa')+L_p(\kappa)+L_p(\kappa')+4}. \tag{9}$$

Thus, we find the energy dependence of the $\mathcal{B}_{\kappa\kappa'}$, $\kappa, \kappa' = 2, \ldots, 12$, to be of the form η^x, with x equal to 6, 7, and 8 for the PsPs, PsPp, and PpPp interference terms, respectively. Here $\eta = q_{\max}/m_\pi$, with $q_{\max}$ being the largest possible value of pion momentum for a given incident energy. By assumption, z_κ, $\kappa = 2, \ldots, 12$, in Eq. (9) are energy-independent complex quantities to be determined from the data.

Since the transition amplitude with the Ss final state does not interfere with any of the other partial waves and since its FSI does not show a power-law behavior [19], we parametrize it as

$$\mathcal{B}_{11}(E_{\text{c.m.}}) = \int_0^{\epsilon_{\max}} |T_1(E_{\text{c.m.}}, \epsilon)|^2\, q(E_{\text{c.m.}}, \epsilon)\, p(\epsilon)\, \mathrm{d}\epsilon = |z_1|^2 \tag{10}$$

and extract it at each of the four bombarding energies individually; $\mathcal{B}_{11}(E_{\text{c.m.}})$ is directly proportional to the bilinear coefficient E in Table IV of Ref. [8].

The values of the coefficients H_1^{00}, H_1^{zz}, F_2, H_2^{Σ}, H_2^{zz}, G_1^{z0}, G_1^{Ξ}, H_1^{z0}, H_2^{z0}, H_4^{Σ}, H_5^{Σ}, H_4^{zz}, and H_5^{zz} were determined by Meyer *et al.* [8] by assuming their energy dependence to be of the form given in Eq. (9). Therefore, in order to be consistent with Ref. [8], we do the following. We plot each of these 13 coefficients as a function of their appropriate η dependence and extract the slope and the corresponding error, using the values and errors in Table IV of Ref. [8]. For example $[\sigma_{\text{tot}}(\eta)F_2(\eta)]/(8\pi^2)$ is plotted against η^6. The values and errors so obtained are then used in our fitting procedure. This gives us a set of 13 equations for the amplitudes z_κ, $\kappa = 2, \ldots, 12$. The remaining 26 coefficients, viz., F_1, H_0^{Σ}, H_0^{zz} and the 23 coefficients from G_1^{y0} to H_5^{Δ}, in Table IV of [8] lead to $26 \times 4 = 104$ equations for the amplitudes z_κ, $\kappa = 2, \ldots, 12$, as they were extracted by [8] without any assumption about their energy dependence. Both the values and errors for these 104 coefficients, taken from Table IV of Ref. [8], were multiplied by $\sigma_{\text{tot}}(\eta)/(8\pi^2)$ for

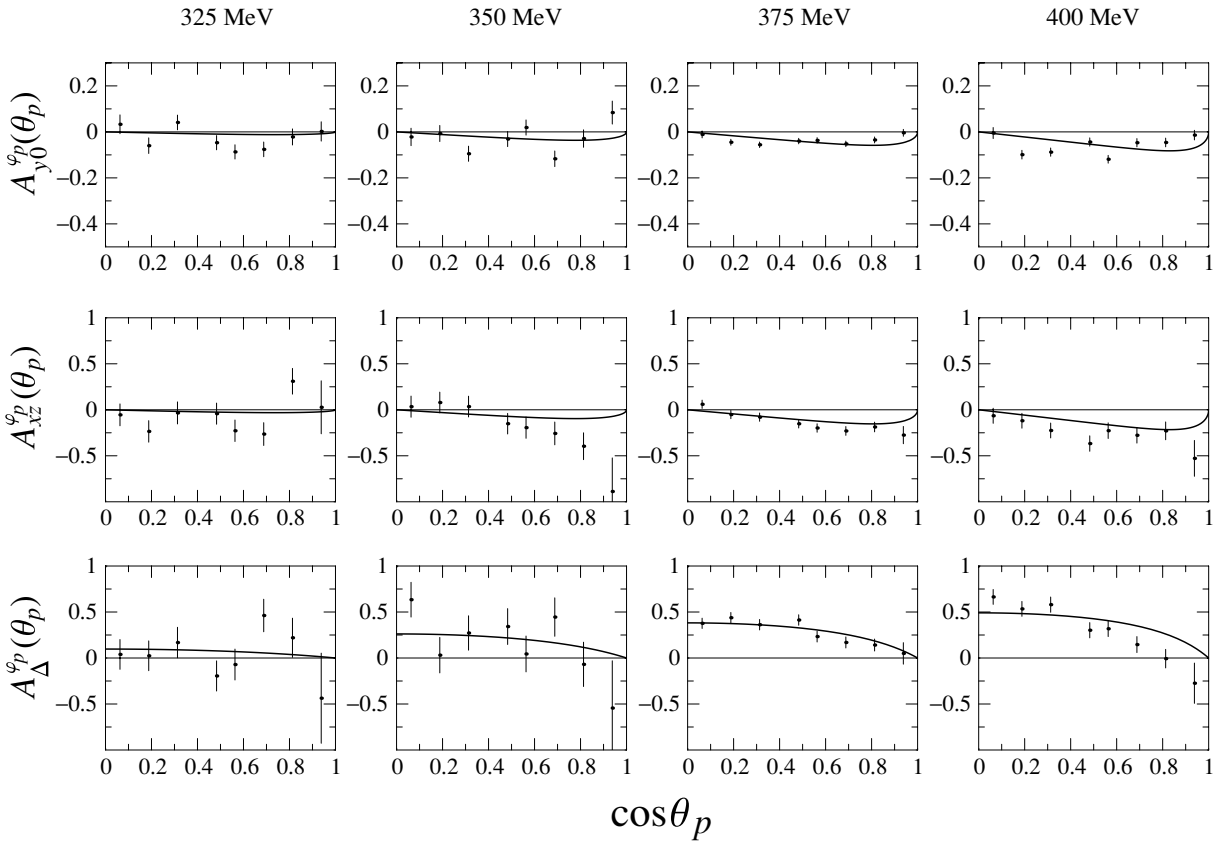

FIG. 4. The observables $A_{y0}^{\varphi_p}(\theta_p)$, $A_{xz}^{\varphi_p}(\theta_p)$, and $A_{\Delta}^{\varphi_p}(\theta_p)$ as a function of the proton angle at several bombarding energies. Same description of data and curves as in Fig. 1.

consistency. In total, we have 117 equations with 21 real unknowns (since z_2 is assumed to be real). In addition, the coefficient E depends only on z_1. Since this amplitude is assumed to be real and we know the explicit dependence of E on z_1, it is directly determined (up to a sign). The uncertainty in z_1 is determined by that in E.

This nonlinear overdetermined system of 117 equations can only have approximate solutions, which were obtained by a χ^2 minimization by using the software MATHEMATICA. The resulting χ^2 per degree of freedom was 1.7. This value was the best that we could obtain after using all four methods of minimization available with MATHEMATICA, viz., differential evolution, Nelder-Mead, random search, and simulated annealing. We performed various checks (different starting vectors setting individual amplitudes to zero) to further support that the minimum is indeed a total minimum. In Figs. 1–6, to illustrate the quality of the fit, we compare our results with some of the observables measured in Ref. [8].

The uncertainties in the z_κ, $\kappa = 2, \ldots, 12$, were determined as follows. Let $\boldsymbol{a}$ denote the vector whose 21 components are the real and imaginary parts of the amplitudes z_i. Then the uncertainty (standard deviation) in any of the components, say a_j, denoted σ_{a_j}, is obtained through [20]

$$\sigma_{a_j}^2 = \sum_{i=1}^{117} \left\{ \sum_{l=1}^{21} \frac{1}{\sigma_i} \left[\epsilon_{jl} \frac{\partial}{\partial a_l} f_i(\boldsymbol{a}) \right]_{\boldsymbol{a}=\boldsymbol{a}_0} \right\}^2. \qquad (11)$$

Here $f_i(\boldsymbol{a})$ stands for the explicit functional form of the bilinear coefficients listed in Table IV of Ref. [8], in terms of the z_κ. σ_i are the corresponding errors in these bilinear coefficients, taken from the same table, and ϵ_{jl} is the (j, l)th element of the error (covariance) matrix $\boldsymbol{\epsilon}$ defined as the inverse of the curvature matrix $\boldsymbol{\alpha}$, whose elements are given by

$$\alpha_{jl} \equiv \frac{1}{2} \frac{\partial^2 \chi^2}{\partial a_j \partial a_l}. \qquad (12)$$

Here $\boldsymbol{a}_0$ is the value of $\boldsymbol{a}$ for which the value of χ^2 is at its minimum.

IV. RESULTS AND DISCUSSION

In Figs. 7 and 8, the values for the z_κ, $\kappa = 1, \ldots, 12$, as determined in the fit are plotted. The uncertainties quoted in these figures for $|z_\kappa|$, $\kappa = 1, \ldots, 12$ and $\tan[\mathrm{Arg}(z_\kappa)]$, $\kappa = 3, \ldots, 12$, were determined by propagating the errors obtained for the real and imaginary parts of the z_κ, $\kappa = 1, \ldots, 12$, in the standard way [21]. It is striking that the amplitude z_2, corresponding to the transition ${}^1S_0 \to {}^3P_0 s$, is the largest.

We now turn to a comparison of the extracted z_κ with the predictions of the microscopic model of the Jülich group. For a detailed description of the model we refer the reader to Refs. [9,12]. Here we only want to summarize its salient features. In the Jülich model all standard pion-production mechanisms [direct production, Fig. 9(a); pion rescattering

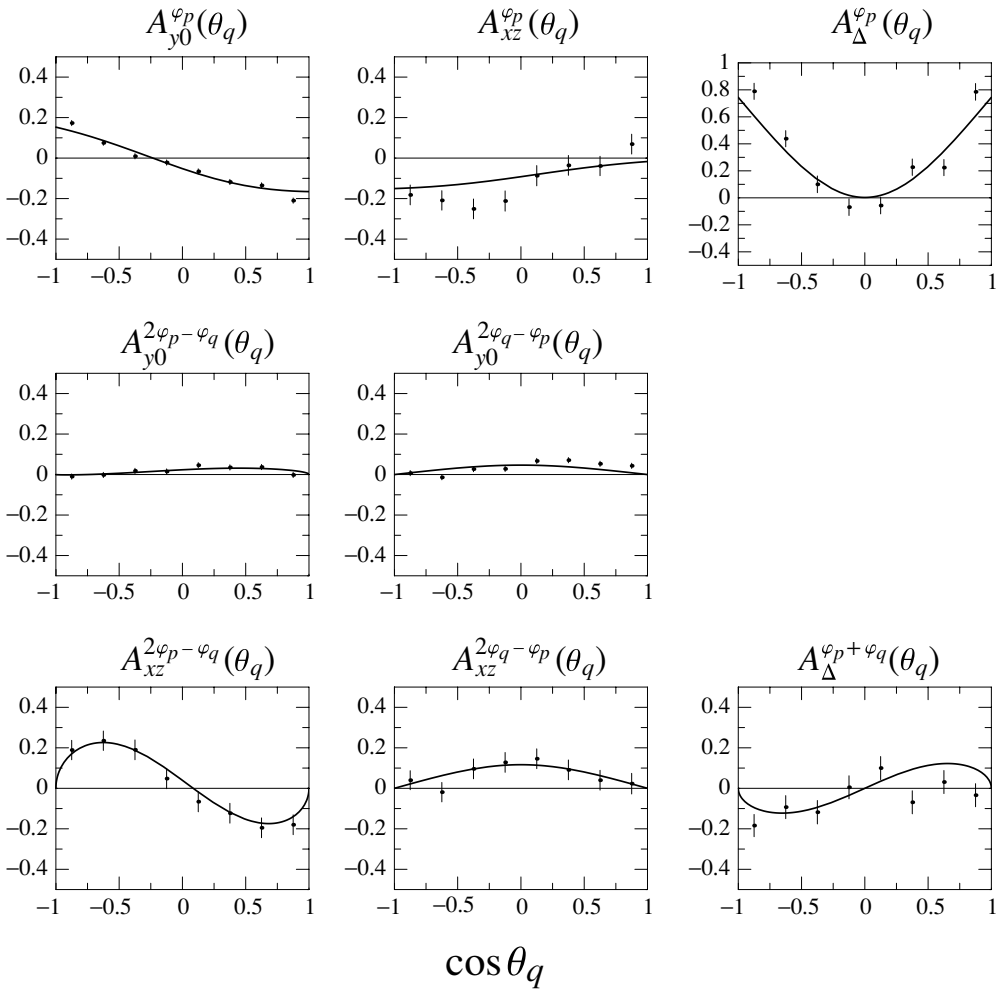

FIG. 5. Additional observables at a bombarding energy of 375 MeV as a function of the pion angle. Same description of data and curves as in Fig. 1.

Fig. 9(b); and contributions from pair diagrams Fig. 9(c)] are considered. In addition, production mechanisms involving the excitation of the $\Delta(1232)$ resonance [cf. Figs. 9(d)–9(g)] are taken into account explicitly. All NN partial waves up to orbital angular momenta $L_p = 2$ and all states with relative orbital angular momentum $l_q \leqslant 2$ between the NN system and the pion are considered in the final state. Furthermore, all πN partial waves up to orbital angular momenta $L_{\pi N} = 1$ are included in calculating the rescattering diagrams in Figs. 9(b), 9(e) and 9(g). Thus, this model includes not only s-wave pion rescattering but also contributions from p-wave rescattering.

The reaction $NN \to NN\pi$ is treated in a distorted-wave Born approximation, in the standard fashion. The actual calculations are carried out in momentum space. For the distortions in the initial and final NN states, a coupled channel (NN, $N\Delta$, $\Delta\Delta$) model is employed [22] that treats the nucleon and the Δ degrees of freedom on equal footing. Thus, the $NN \leftrightarrow N\Delta$ transition amplitudes and the NNT matrices that enter in the evaluation of the pion-production diagrams in Fig. 9 are consistent solutions of the same (coupled-channel) Lippmann-Schwinger-like equation.

By taking the partial-wave amplitudes $T_\kappa(E_{\text{c.m.}}, \epsilon)$ predicted by the model, it is straightforward to extract the moduli of the z_κ from the model through their definition in Eqs. (7) and (9):

$$\left|z_\kappa^{\text{model}}\right| = \eta^{-l_q(\kappa)-L_p(\kappa)-2}\sqrt{\mathcal{B}_{\kappa\kappa}(E_{\text{c.m.}})}.$$

Since the phases of the bilinears $\mathcal{B}_{\kappa\kappa'}$ calculated from the model are not in all cases consistent with the factorization used in Eq. (9), they cannot be compared easily with those extracted from the data.

The $|z_\kappa|$ predicted by the model are compared with the results of the partial-wave analysis in Fig. 10. In the upper part of the graph we compare the moduli of the z_κ of the model with those obtained by our partial-wave analysis, while in the lower part the deviation of the model predictions from the analysis are presented. Note that the model results are normalized in such a way that $|z_1|$ for a bombarding energy of 375 MeV (i.e., the one corresponding to the ${}^3P_0 \to {}^1S_0 s$ transition) coincides with the corresponding extracted value. This is done in order to facilitate the comparison between the various other $|z_\kappa|$.

It is evident from Fig. 10 that the microscopic model of Refs. [9,12] yields a rather impressive overall description of

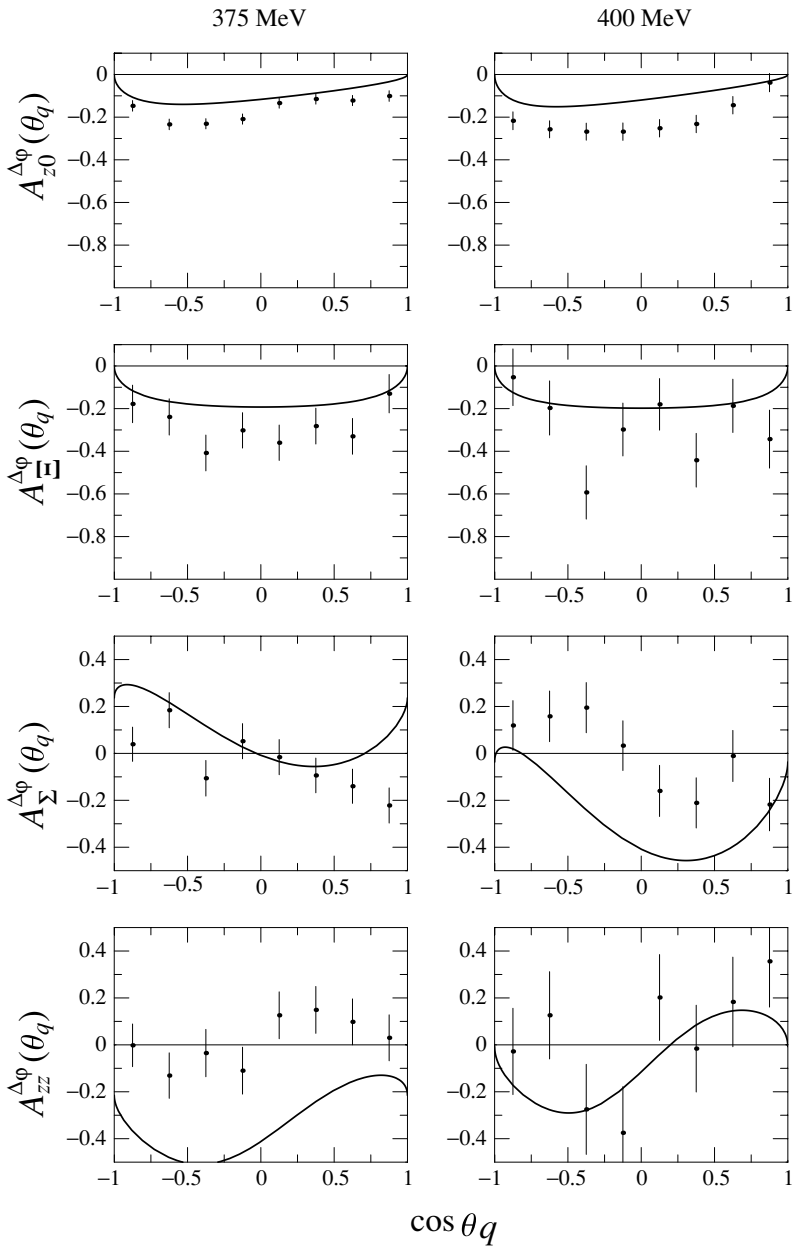

FIG. 6. Observables that depend on $\Delta\varphi$, plotted as a function of the angle θ_q at the bombarding energies of 375 and 400 MeV, at which the measurement of Ref. [8] has the best statistics. Same description of data and curves as in Fig. 1.

the various partial-wave amplitudes; cf. the squares and circles. This is particularly remarkable because one has to keep in mind that practically all parameters of the model were fixed by other reactions (elastic NN scattering and πN scattering).[2] In fact the majority of the partial-wave amplitudes is reproduced even quantitatively (if one takes into account the error bars of the partial-wave analysis). The only serious discrepancy occurs in the amplitude z_9 ($^3P_1 \to {}^3S_1 p$) and to a lesser extent also in z_{12} ($^3F_3 \to {}^3P_0 p$). The reason for the shortcoming in the model prediction for these $|z_\kappa|$ and the connection with its dynamical ingredients needs to be explored in the future.

Figure 10 also suggests considerable deviations in z_{13}, z_{15}, and especially z_{16}. However, these z_κ correspond to partial waves with $NN\,D$ waves or pion d waves in the final state whose contribution had been set to zero in the analysis of Meyer *et al*. [8]—as well as in ours—as already mentioned above. Thus, the predictions of the microscopic model can be seen as an indication that those amplitudes are likely not negligible and therefore should be taken into account in any future analysis of the reaction $pp \to pp\pi^0$. Since in the present analysis the neglected contributions of the D-wave and d-wave amplitudes are presumably mimicked by other partial-wave amplitudes, a more complete partial-wave analysis could yield results that are even closer to the model prediction than for the case considered in the present paper.

While a well-founded theoretical interpretation of the obtained partial-wave amplitudes calls for a thorough investigation, e.g., within the framework of effective field theory, as advocated in Refs. [2,4,5], the presented analysis already

[2]The only free parameter was fixed to the total cross section for $pp \to pp\pi^0$ at low energies [11].

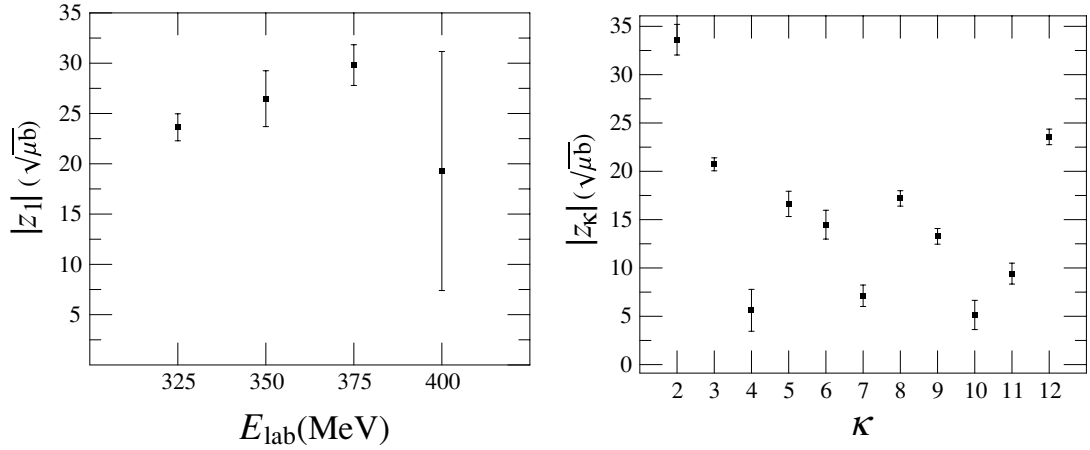

FIG. 7. Left panel: Moduli [in $(\mu b)^{1/2}$] of z_1 for bombarding energies E_{lab} of 325, 350, 375, and 400 MeV. Right panel: Moduli [in $(\mu b)^{1/2}$] of the z_κ, $\kappa = 2, \ldots, 12$.

allows us to shed light on the role of the Δ (1232) resonance for π^0 production. The importance of the Δ isobar for the reaction $NN \to NN\pi$ was already pointed out in Ref. [9]. The present partial-wave analysis allows us to confirm that aspect nicely in a quantitative and transparent way. The results of the model of Refs. [9,12] after omitting contributions involving Δ degrees of freedom are shown by the triangles in Fig. 10. The corresponding predictions clearly fall short in describing the amplitudes of the partial-wave analysis. In particular, even the qualitative trend in the magnitude of the amplitude is not reproduced.

Further insight can be gained by taking into account only those $NN \to N\Delta$ transitions that occur before the pion emission [Figs. 9(d) and 9(e)]. The corresponding predictions for the $|z_\kappa|$ are shown by the open diamonds in Fig. 10. For almost all partial waves this part provides the dominant Δ effect, as expected, since the energy of the incoming NN system is not too far away from the nominal $N\Delta$ threshold. The energy in the outgoing NN system, on the other hand, is much smaller and therefore the excitation of the $\Delta(1232)$ is expected to be of much less significance. However, to achieve also a quantitative agreement with the extracted $|z_\kappa|$, the Δ excitation in the final state [after pion emission: Figs. 9(f) and 9(g)] is essential, as can be most clearly seen in case of z_2 ($^1S_0 \to {}^3P_0 s$) and z_3 ($^1D_2 \to {}^3P_2 s$). Specifically, only after inclusion of the Δ in the final state does the former became larger than the latter.

In this context it is also important to note that both types of contribution, the emission of a real pion from a Δ decay—as depicted in diagrams (d) and (f) of Fig. 9—and the emission of a virtual pion from a Δ that becomes rescattered off the other nucleon—depicted in diagrams (e) and (g) of Fig. 9—are of similar numerical significance. This should not come as a surprise, for as soon as the Delta isobar is involved, the large isovector pion nucleon interaction can contribute to the neutral pion production [12]. This is also consistent with the fact that both these contributions (among others) contribute at next-to-leading order in the chiral expansion [5].

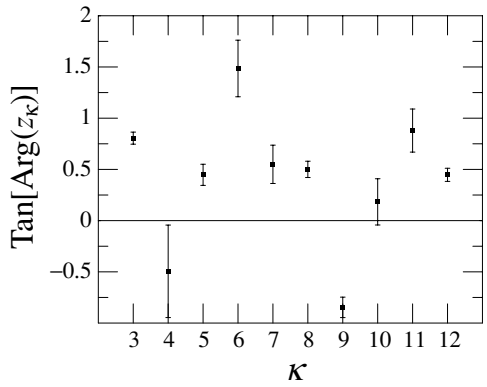

FIG. 8. Tangent of the arguments of the z_κ, $\kappa = 3, \ldots, 12$.

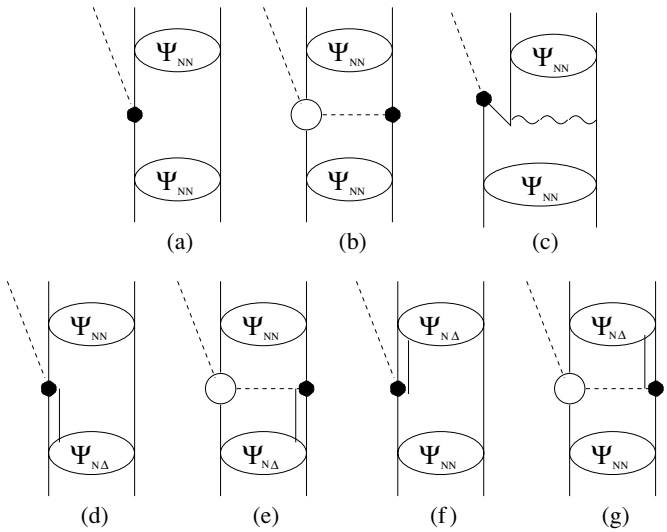

FIG. 9. Pion-production mechanisms taken into account in the model of Ref. [9]: (a) direct production; (b) pion rescattering; (c) contributions from pair diagrams; (d) to (g) production involving the excitation of the $\Delta(1232)$ resonance, depicted by the double line. In the diagrams the pion (nucleon) is shown as a dashed (solid) line.

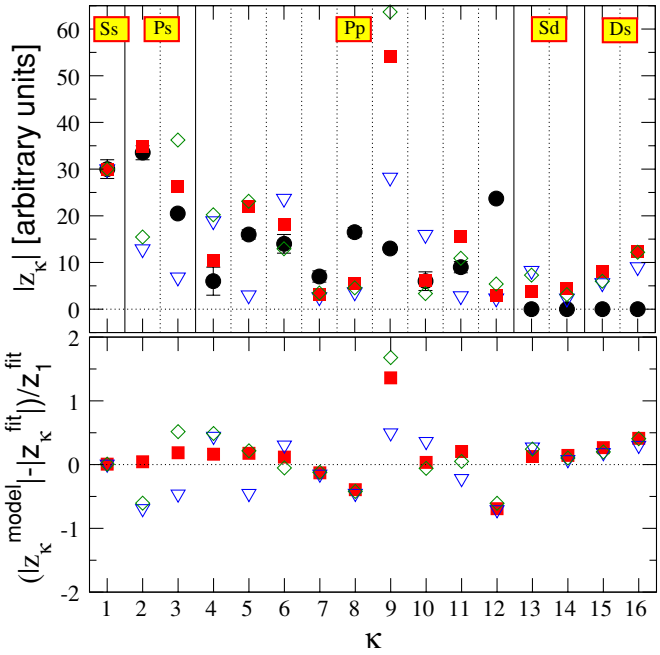

FIG. 10. (Color online) Comparison of the extracted $|z_\kappa|$ (filled circles) to the corresponding quantities predicted by the microscopic model of Ref. [9] (filled squares). The inverted triangles show results where the Δ contributions of the model were omitted completely, whereas the diamonds represent results of a calculation where only the Δ contributions after pion emission were omitted. In the upper panel the results for the various $|z_\kappa|$ are shown, normalized with respect to our extracted value for $|z_1|$ at 375 MeV, while in the lower panel the relative deviations of the model calculation from the extracted values are shown.

In any case, it should be clear from this discussion that the Δ degrees of freedom have to be taken into account explicitly in any model that aims at a quantitative description of the reaction $pp \to pp\pi^0$, even for energies near the pion-production threshold.

V. SUMMARY AND OUTLOOK

We have presented a partial-wave analysis of the double polarization data for the reaction $pp \to pp\pi^0$, measured at the IUCF [8]. Due to the limited statistical accuracy of the data, following the authors of Ref. [8], we made several assumptions about the contributing amplitudes in order to be able to perform the analysis. The quality of the fit, with a χ^2 per degree of freedom of 1.7, is not completely satisfying. This could be a consequence of the assumptions that were made in the analysis.

When compared with the results of a microscopic model [9], the analysis made three important points rather explicit: (i) the Δ degree of freedom is important for a quantitative understanding of the reaction $pp \to pp\pi^0$, (ii) there is especially one z_κ that very strongly deviates from that extracted from the data, namely z_9 ($^3P_1 \to {}^3P_0 p$)—this will guide the search for the possible short-comings of the model, and (iii) the set of partial waves included in the analysis was possibly too limited.

As a next major step a combined analysis of *NN* scattering data and data on $NN \to NN\pi$ needs to be performed. On the one hand, the pion production channels directly provide the inelasticities to be used for the analysis of the *NN* data; on the other hand, the *NN* elastic phase shifts provide the phase motion as well as the dominant energy dependence of the moduli of the production amplitudes. The latter connection is provided by dispersion integrals as discussed in detail in Refs. [2,22].

ACKNOWLEDGMENTS

We acknowledge helpful communication with H. O. Meyer and L. Knutson. Furthermore, we thank Ulf-G. Meiβner for a careful reading of the manuscript. P.N.D. acknowledges with thanks the support of the Alexander-von-Humboldt Foundation.

[1] P. Moskal *et al.*, Prog. Part. Nucl. Phys. **49**, 1 (2002).
[2] C. Hanhart, Phys. Rep. **397**, 155 (2004).
[3] V. Bernard, N. Kaiser, and U.-G. Meißner, Int. J. Mod. Phys. E **4**, 193 (1995).
[4] C. Hanhart, U. van Kolck, and G. A. Miller, Phys. Rev. Lett. **85**, 2905 (2000).
[5] C. Hanhart and N. Kaiser, Phys. Rev. C **66**, 054005 (2002).
[6] A. K. Opper *et al.*, Phys. Rev. Lett. **91**, 212302 (2003).
[7] E. J. Stephenson *et al.*, Phys. Rev. Lett. **91**, 142302 (2003).
[8] H. O. Meyer *et al.*, Phys. Rev. C **63**, 064002 (2001).
[9] C. Hanhart, J. Haidenbauer, O. Krehl, and J. Speth, Phys. Lett. **B444**, 25 (1998).
[10] Y. Maeda, N. Matsuoka, and K. Tamura, Nucl. Phys. **A684**, 392 (2001).
[11] C. Hanhart, J. Haidenbauer, A. Reuber, C. Schütz, and J. Speth, Phys. Lett. **B358**, 21 (1995).
[12] C. Hanhart, J. Haidenbauer, O. Krehl, and J. Speth, Phys. Rev. C **61**, 064008 (2000).
[13] W. W. Daehnick *et al.*, Phys. Rev. C **65**, 024003 (2002).
[14] B. v. Przewoski *et al.*, Phys. Rev. C **61**, 064604 (2000).
[15] G. Ramachandran, P. N. Deepak, and M. S. Vidya, Phys. Rev. C **62**, 011001(R) (2000).
[16] G. Ramachandran and M. S. Vidya, Phys. Rev. C **56**, R12 (1997).
[17] M. Goldberger and K. M. Watson, *Collision Theory* (Wiley, New York, 1964).
[18] A. H. Rosenfeld, Phys. Rev. **96**, 1 (1954).
[19] G. A. Miller and P. U. Sauer, Phys. Rev. C **44**, 1725(R) (1991).
[20] K. H. Burrell, Am. J. Phys. **58** (2), 160 (1990).
[21] P. R. Bevington, *Data Reduction and Error Analysis for the Physical Sciences* (McGraw-Hill, New York, 1969), p. 60, Eqs. (4–9).
[22] J. Haidenbauer, K. Holinde, and M. B. Johnson, Phys. Rev. C **48**, 2190 (1993).